SIAM J. Applied Dynamical Systems
Vol. 14, No. 4, pp. 2013–2029

Bifurcations in Forced Response Curves*

Justin Wiser† and Martin Golubitsky‡

Abstract. We consider small amplitude periodic forcing (with forcing frequency ω_F) of a system of differential equations near a point of Hopf bifurcation (with Hopf frequency ω_H). We follow Zhang and Golubitsky [*SIAM J. Appl. Dyn. Syst.*, 10 (2011), pp. 1272–1306] and consider only those small amplitude periodic solutions to the forced system whose frequency is ω_F; that is, the 1:1 phase-locked or entrained solutions. These authors assume sinusoidal forcing of a normal form Hopf system when ω_F is close to ω_H, and they classify the existence and multiplicity of the entrained solutions. The *forced response curve* is a bifurcation diagram showing the amplitude of the entrained solutions as the forcing frequency is varied. Zhang and Golubitsky showed that there are six kinds of forced response curves with distinguished bifurcation parameter $\omega = \omega_H - \omega_F$. In this paper we show that there are 41 possible bifurcation diagrams when stability in addition to multiplicity of the periodic solutions in the forced response curves is included.

Key words. Hopf bifurcation, periodic forcing, resonance

AMS subject classifications. 34C23, 34C25, 34F15, 37G15

DOI. 10.1137/14096846X

1. Introduction.

Resonant responses to periodically forced nonlinear dynamical systems have been studied extensively. Indeed, complicated or chaotic dynamics may occur in regions of parameter space outside of *m:n Arnold tongues* where m periods of the external forcing drive n periods of the forced response. See, for example Arnold [1, 2] or Broer [5] and the references therein. In this paper, we study periodic solutions to forced Hopf oscillators that are 1:1 phase-locked (or *entrained*) with an external, periodic forcing.

There are numerous examples of periodically forced systems near Hopf bifurcations in the applied math and engineering literature. Band pass filters are electrical devices that may be tuned near Hopf bifurcations to amplify electrical signals in a frequency selective way (Mees and Chua [16]; Simpson [17]; McCullen, Mullin, and Golubitsky [15]). Biochemical oscillators may similarly be tuned near Hopf bifurcation points, adding frequency selectivity to larger signal transduction cascades and allowing a pathway to selectively respond to an oscillatory chemical messenger (Tyson [18], Wiser [19]). Neurons tuned near Hopf bifurcations may play a role in sensory perception (Baier and Müller [3], Balakrishnan and Ashok [4]), and hair bundles tuned near Hopf bifurcations may play a role in cochlear dynamics (Hudspeth [13]), again affording these systems frequency selectivity and response amplification when the forcing is near the Hopf frequency.

*Received by the editors May 9, 2014; accepted for publication (in revised form) by B. Sandstede September 30, 2015; published electronically November 19, 2015. This research was supported in part by NSF grant DMS-D931642 to the Mathematical Biosciences Institute.
http://www.siam.org/journals/siads/14-4/96846.html
†Department of Mathematics, The Ohio State University, Columbus, OH 43210 (jwiser84@gmail.com).
‡Mathematical Biosciences Institute, The Ohio State University, Columbus, OH 43210 (mg@mbi.osu.edu). The research of this author was supported in part by NSF grant DMS-1008412.

Mathematically, the problem of periodically forced systems near Hopf bifurcations has been addressed by numerous authors. Many have studied specific examples of forced systems with Hopf bifurcations. Gambaudo [8] studied periodically forced Hopf bifurcation and found the response of such a system in a very general setting as well as how this response may change if one varied model parameters. However, the ubiquity of frequency selectivity in the applications above suggests that studying periodically forced Hopf bifurcation as a distinguished parameter bifurcation problem in the forcing frequency (i.e., classifying the forced response of nonlinear resonant systems) may help shed light on numerous models of physical systems.

Definition 1.1. *The* forced response curve *is a graph showing the amplitude of the response of a periodically forced system as the forcing frequency is varied. The* response *is a periodic solution that is* 1:1 *phase-locked with the forcing frequency.*

Zhang and Golubitsky [20] studied the structure of forced response curves in periodically forced systems near a point of Hopf bifurcation and how these curves change as one varies model parameters (see Figure 1). In this paper we discuss both the existence and stability of solutions enumerated by the forced response curves.

We may describe the results in [20] as follows. First, we restrict our attention to truncated third order Hopf normal form written in complex notation (although their analysis was conducted in a more general setting) and assume small amplitude simple sinusoidal forcing to obtain the system

$$\frac{dz}{dt} = (\lambda + i\omega_H)z \pm (1 + i\gamma)|z|^2 z + \varepsilon e^{i\omega_F t}, \tag{1.1}$$

where $\pm$ is chosen to be $+$ for a periodically forced subcritical oscillator and $-$ for a periodically forced supercritical oscillator, ω_H is the Hopf frequency, ω_F is the forcing frequency, and γ is the ratio of the imaginary to real parts of the cubic coefficient (the system may be rescaled to take this form provided the real part is nonzero). Here the system is subjected to sinusoidal forcing with small amplitude given by ε.

For fixed γ, Zhang and Golubitsky determined the forced response curves (for $\omega_F \approx \omega_H$) and their transitions for $\lambda \approx 0$ and small $\varepsilon > 0$. We show in Lemma 2.1 that (1.1) can be rescaled so that $\varepsilon = 1$ in such a way as to preserve the structure of the forced response curves and their transitions. When we do this, we can summarize the results of [20] in Figure 1. For example, [20] showed that there can be hysteresis in the forced response curve (so that the response amplitudes may depend on whether the forcing frequency is increasing or decreasing) and that the forced response curve may bifurcate (creating isolas of solutions that may not be noticed experimentally or numerically if the system were subjected only to small parametric variation). However, missing from their analysis is a study of the stability of the periodic solutions that correspond to points on the forced response curves. This information is necessary for applications and is the subject of this paper.

Calculating the stability of periodic solutions corresponding to points on the forced response curve allows us to show the existence of several new bifurcations and several additional types of solutions. It is natural to discuss these solutions in rotating coordinates, rotating with frequency ω_F. In rotating coordinates the periodic forced response is given by a fixed point. The new bifurcations include the following:

- Secondary Hopf bifurcations (i.e., Hopf bifurcation of fixed points in rotating coor-

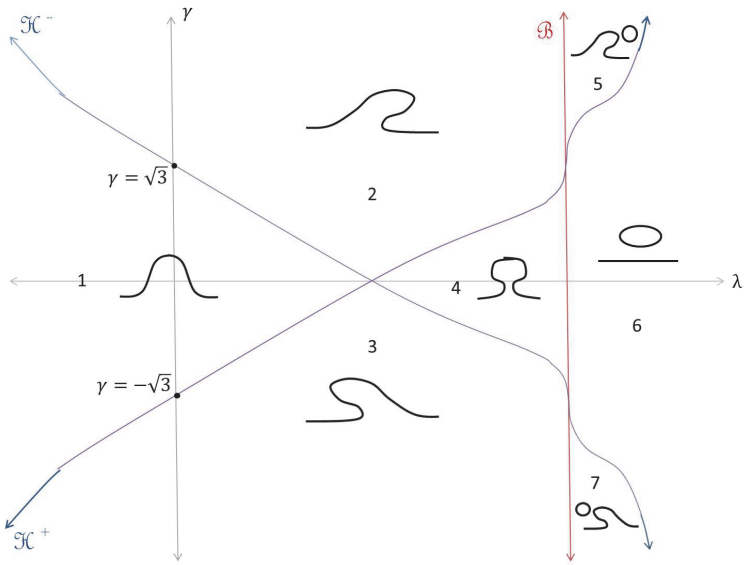

Figure 1. *Forced response curves of the system* (1.1). *Each curve shows the amplitude of the forced response as a function of* $\omega = \omega_H - \omega_F$. *The hysteresis varieties cross* $\lambda = 0$ *transversely and the bifurcation varieties with a cubic tangency when* $\gamma = \pm\sqrt{3}$.

dinates) where the periodic forced response can exchange stability and give rise to a branch of tori.

- Takens–Bogdanov points where these branches of secondary Hopf bifurcation can terminate and where branches of homoclinic connections exist.
- Degenerate secondary Hopf bifurcations can occur.
- A homoclinic connection may terminate when its point of origin undergoes a saddle node bifurcation.

These dynamics give rise to more regions than are shown in Figure 1. In Figure 2 we have added six transition varieties: $TB^{\pm}$ are Takens–Bogdanov varieties, $CC^{\pm}$ are change of criticality curves corresponding to degenerate secondary Hopf bifurcations, and $SNL^{\pm}$ indicate the termination of homoclinic connections (local to the TB varieties) following a connection to a degenerate saddle point.

We then draw forced response curves with dynamical information encoded that correspond to each of these regions. See Figure 3. Here the dark blue portions of the curve indicate stable periodic solutions, and the light blue portions indicate unstable solutions. The red portions indicate saddle points. The transitions from red to black indicate saddle node bifurcations. The transitions from light blue to dark blue indicate secondary Hopf bifurcation. When denoted by a dark (light) blue dot, this indicates that the secondary Hopf bifurcation is supercritical (subcritical). The dark (light) branch emanating from the secondary Hopf bifurcations denotes a branch of stable (unstable) tori. The presence of tori is seen in practice as the onset of a secondary frequency, or an amplitude modulating frequency. The tori may terminate via homoclinic bifurcation (where the period of the secondary oscillations tends to ∞). The presence of a homoclinic connection is denoted by an "X" over the saddle point to which

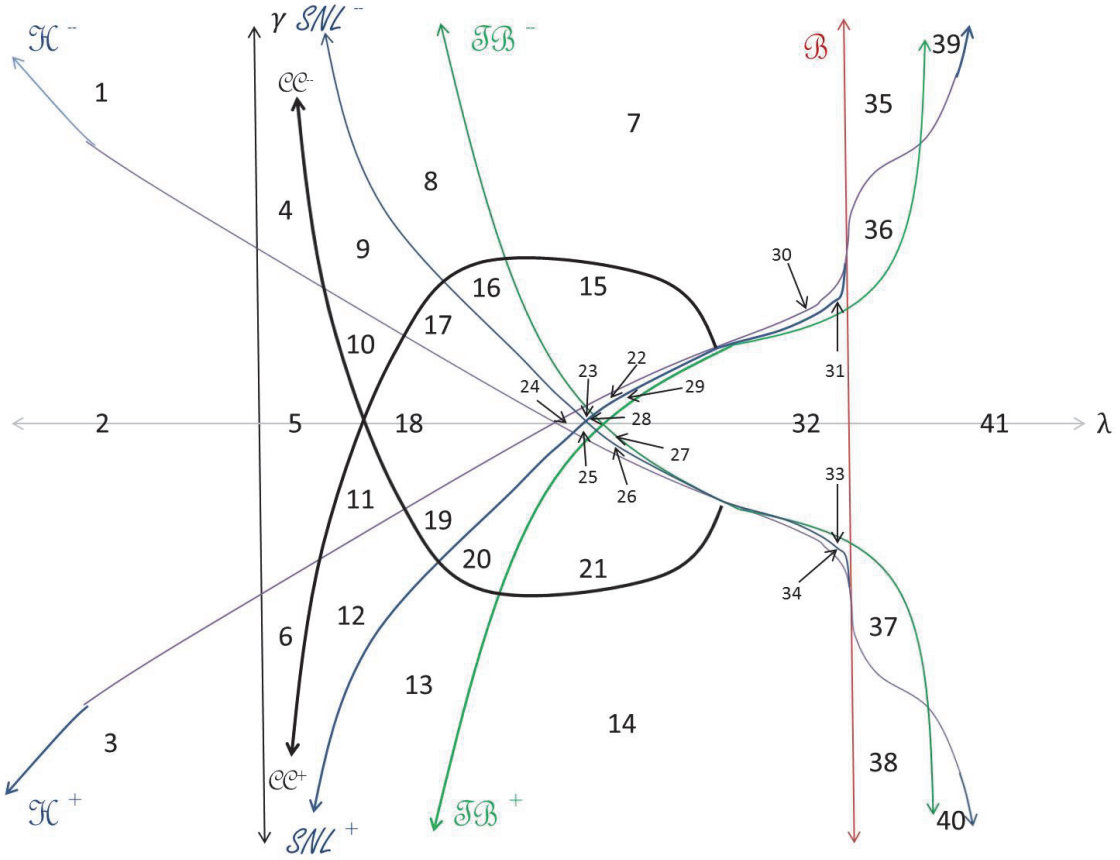

Figure 2. *Here we have added six transition varieties: $TB^{\pm}$ are Takens–Bogdanov varieties, $CC^{\pm}$ are change of criticality curves corresponding to degenerate secondary Hopf bifurcations, and $SNL^{\pm}$ indicate the termination of homoclinic connections (local to the TB varieties) following a connection to a degenerate saddle point. The regions have been renumbered, and the forced response curves for each region, in all detail, are given in Figure 3. Note that $\mathcal{CC}^{\pm}$ curves are drawn differently than they actually are in order to make the diagram easier to read. Actually $\mathcal{CC}^{+}$ implicitly defines γ as a monotonically increasing function of λ, and $\mathcal{CC}^{-}$ defines γ as a monotonically decreasing function of λ.*

the connection exists. If it is dark (light) blue, this indicates that it is a stable (unstable) homoclinic orbit. The diagrams shown are for a periodically forced supercritical Hopf normal form. One may easily alter these diagrams to understand the dynamics of a periodically forced subcritical normal form (see [19]).

We should also recall that these diagrams only show the dynamics of a fully entrained forced response. In practice, regions of instability could also result from entering regions of parameter space on a higher order $m : n$ Arnold tongue.

To summarize, in Figure 3, black lines indicate a stable equilibrium, red lines indicate saddle points, and light blue lines indicate an unstable equilibrium. Red/black and red/blue boundaries indicate a saddle node bifurcation. Black/blue boundaries indicate a secondary

Hopf bifurcation and are accompanied by a dot (dark blue for supercritical Hopf bifurcations and light green for subcritical) and a line indicating the direction of branching periodic orbits.

In practice, it is rarely important to understand all of the transitions in this diagram or where they occur as some model parameters are varied. However, it is extremely convenient that the transitions one expects to see as one varies parameters can be determined by a computation of a single parameter γ at the Hopf bifurcation point. A formula for γ and Mathematica code for its computation are given in [19].

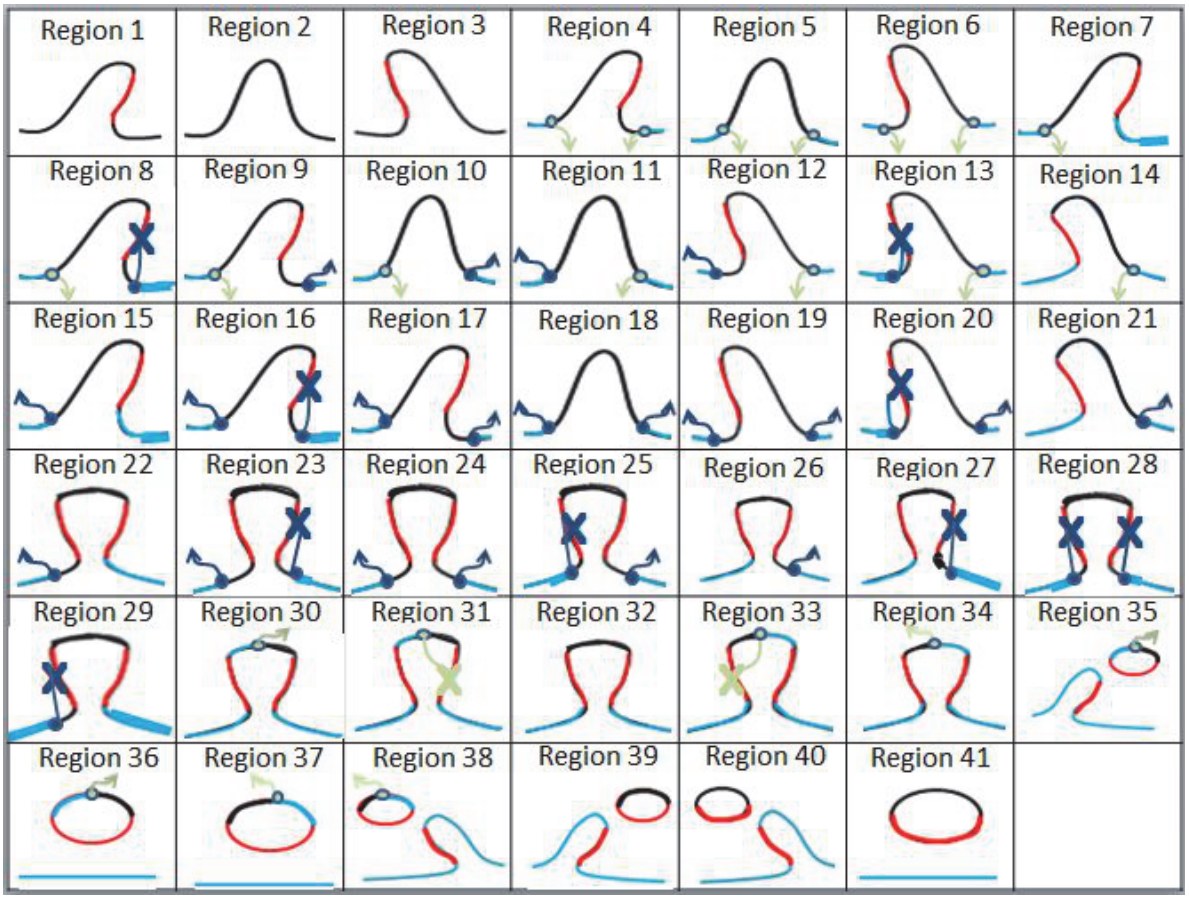

Figure 3. *Forced response curves for regions shown in Figure 2.*

The first section of this paper will be devoted to establishing the results summarized in Figures 2 and 3. The second part of this paper will be devoted to determining the generality of this result. Although coordinate changes may be used to put a system with a Hopf bifurcation into normal form up to third order, we investigate the effects of truncating higher order terms. Also, while we will not attempt to fully generalize the forcing term to include nonsinusoidal forcing, we have considered taking a periodically forced system with a Hopf bifurcation and introducing coordinate changes to put the system in normal form. The effect of these coordinate changes on the forcing cannot be ignored. We find a class of generalizations (which we call *separable forcing*), which includes the complexities discussed above (as well as many other

types of forcing—most notably, parametric forcing) and find that the diagrams in Figures 2 and 3 describe these systems as well.

2. Periodically forced, third order Hopf normal form. In this section, we will study the supercritical Hopf normal form, truncated to third order, subjected to an external sinusoidal forcing

$$\frac{du}{dt} = (\lambda + i\omega_H)u \pm (\alpha + i\beta)|z|^2 z + \varepsilon e^{i\omega_F t} \tag{2.1}$$

(where $\alpha < 0$) without concern about the generality of the results obtained, which will be discussed in the next section. We begin with the results of Zhang and Golubitsky shown in Figure 1 and begin to derive stability results. We note that Figure 1 does not appear in [20]. The bifurcation diagrams in [20] were given in $\mathbf{R}^3$ since the system was not rescaled to eliminate ε.

2.1. Rotating coordinates and a rescaling. We begin by looking at (2.1) in a coordinate system rotating with frequency ω_F using the variable

$$z = ue^{i\omega_F t}.$$

The system then becomes autonomous,

$$\dot{z} = (\lambda + i\omega)z - (\alpha + i\beta)|z|^2 z + \varepsilon, \tag{2.2}$$

where $\omega = \omega_H - \omega_F$. Next, we reduce the number of parameters by rescaling.

Lemma 2.1. *The system* (2.2) *may be rescaled to have the form*

$$\dot{z} = (\lambda + i\omega)z - (1 + i\gamma)|z|^2 z + 1. \tag{2.3}$$

Proof. We introduce the rescaling

$$t = \alpha\tau, \quad \hat{z} = \alpha z, \quad \hat{\lambda} = \alpha\lambda, \quad \hat{\omega} = \alpha\omega, \quad \gamma = \frac{\beta}{\alpha}, \quad \hat{\varepsilon} = \alpha^2\varepsilon.$$

Rewriting the system in this form, dropping the "hats," we obtain

$$\dot{z} = (\lambda + i\omega)z - (1 + i\gamma)|z|^2 z + \varepsilon. \tag{2.4}$$

Next, we rescale small parameters using powers of ε via

$$z = \hat{z}\varepsilon^{\frac{1}{3}}, \quad \lambda = \hat{\lambda}\varepsilon^{\frac{2}{3}}, \quad \omega = \hat{\omega}\varepsilon^{\frac{2}{3}}, \quad t = \tau\varepsilon^{\frac{2}{3}}, \tag{2.5}$$

and writing the system in these coordinates (and dropping the "hats"), we obtain (2.3). ∎

We then attempt to produce the bifurcation diagram in Figure 1 for the systems (2.4) and (2.3).

Lemma 2.2. *As shown in* [20]*, periodic solutions to* (2.4) *correspond to zeros of*

$$H(R) = (1 + \gamma^2)R^3 - 2(\lambda + \gamma\omega)R^2 + (\lambda^2 + \omega^2)R - \varepsilon^2 = 0, \tag{2.6}$$

where $R = |z|^2$.

Proof. We will follow the derivation of (1.8) in [20] in truncated normal form to arrive at the desired result. Setting $\dot{z} = 0$ in (2.4), we find that

$$(\lambda + i\omega - (1 + i\gamma)|z|^2)z = -\varepsilon. \tag{2.7}$$

Separating the first factor on the left-hand side of (2.7) into real and imaginary parts, we obtain

$$((\lambda - |z|^2) + i(\omega - \gamma|z|^2))z = -\varepsilon.$$

Finally, substituting $R = |z|^2$, we may simplify:

$$((\lambda - R) + i(\omega - \gamma R))z = -\varepsilon.$$

Taking the norm squared of both sides, we arrive at the desired result. ∎

Thus, the number of solutions to the algebraic equation (2.6) correspond to the number of periodic solutions of (2.4) with the same parameter values. Also, since $R = |z|^2$, the value of the solutions to (2.6) gives a measure of the amplitude of the periodic solutions to (2.4).

If we consider $H(R) = 0$ as a bifurcation diagram with ω as a distinguished parameter and γ, λ, and ε as unfolding parameters, then singularity theory enumerates the ways that such a diagram may be nonpersistent (i.e., may qualitatively change if subjected to a small perturbation) [9, p. 140]. That is, in parameter space one may encounter a simple bifurcation variety,

$$\mathcal{B} = \{(\gamma, \lambda, \varepsilon) : H = H_R = H_\omega = 0 \quad \text{for some} \quad R, \omega\}.$$

This defines a codimension 1 surface in $(\lambda, \gamma, \varepsilon)$ space. One may also encounter a hysteresis variety,

$$\mathcal{H} = \{(\gamma, \lambda, \varepsilon) : H = H_R = H_{RR} = 0 \quad \text{for some} \quad R, \omega\},$$

also defining a codimension 1 surface in $(\lambda, \gamma, \varepsilon)$ space. Note that, generally, there is a third possibility that one may find a double limit point variety $\mathcal{D}$, which we will not define. Since H is third order in R, $\mathcal{D}$ is empty (see [9, pg. 148]). We may then define the transition variety $\mathcal{T} = \mathcal{B} \cup \mathcal{H}$. On connected components of the complement to $\mathcal{T}$ in $(\lambda, \gamma, \varepsilon)$ space, the curves giving solutions to $H(R) = 0$ as a function of ω are persistent as distinguished parameter bifurcation diagrams.

Bifurcation and hysteresis varieties were found in the analysis of (2.6) by Zhang and Golubitsky in [20]. There is one simple bifurcation variety $\mathcal{B}$, given by

$$\lambda^3 = \frac{27}{4}\varepsilon^2, \tag{2.8}$$

and two hysteresis varieties, $\mathcal{H}^+$ and $\mathcal{H}^-$, given by

$$\lambda^3 = \frac{(3 \pm \sqrt{3}\gamma)^3}{8(1 + \gamma^2)}\varepsilon^2. \tag{2.9}$$

These varieties are all local since they tend to the origin as $\varepsilon \to 0$. However, when we introduce the rescaling, (2.5), and write the system in these coordinates (dropping the "hats"), we obtain not only our rescaled version of (2.4)

$$\dot{z} = (\lambda + i\omega_H)z - (1 + i\gamma)|z|^2 z + 1 \tag{2.10}$$

but also a rescaled version of (2.6):

$$H(R) = (1+\gamma^2)R^3 - 2(\lambda+\gamma\omega)R^2 + (\lambda^2+\omega^2)R - 1 = 0. \tag{2.11}$$

This reduces the number of parameters in the bifurcation problem by eliminating ε.

We may then collect the above information about the bifurcation diagrams in ω by sketching the varieties $\mathcal{B}$, $\mathcal{H}^+$, and $\mathcal{H}^-$ in the (λ,γ) plane and obtain the curves shown in Figure 1. However, we still must determine which bifurcation diagrams in ω we see as we traverse (λ,γ) space. To start, we determine what happens when one crosses the hysteresis varieties. Specifically, we would like to know if our system provides a universal unfolding of the hysteresis degeneracy and, if so, the direction in which the forced response curve "tips over" when we cross the hysteresis variety.

Proposition 2.3. *If we tune the system (2.4) to a hysteresis point in ω, then variation of λ produces a universal unfolding of the hysteresis point provided $\varepsilon > 0$. Furthermore, if we refer to the first hysteresis point (as λ increases from 0) as $\mathcal{H}^-$ and the second as $\mathcal{H}^+$, the direction of the hysteresis folding is as shown in Figure 1 in (Regions 2, 3, and 4).*

This result can easily be seen numerically. A proof can be found in [19]. With this information, we may fill in the bifurcation diagrams in Regions 1, 2, and 3 of (λ,γ) parameter space (see Figure 1). Comparing the bifurcation diagrams in Regions 2 and 3, we may also determine the bifurcation diagram in Region 4. To determine the bifurcation diagrams in the rest of the regions, we prove the following proposition.

Proposition 2.4. *At the intersection of the bifurcation and the hysteresis varieties in the unfolding of the periodically forced Hopf oscillator in rotating coordinates (2.3), i.e., when $\gamma = \pm\sqrt{3}$, there is a pitchfork bifurcation in the distinguished parameter ω. Additionally, perturbations of the pitchfork bifurcations in (λ,γ) parameter space give a universal unfolding of the pitchfork.*

Proof. The defining conditions for the simple bifurcation variety are given by $H = H_R = H_\omega = 0$. The defining conditions for the hysteresis variety are $H = H_R = H_{RR} = 0$. So, $H = H_R = H_{RR} = H_\omega = 0$ must be satisfied at the intersection. Thus, H(R) meets the defining conditions for a pitchfork bifurcation in the parameter ω. We must check that the nondegeneracy conditions are satisfied. We check that $H_{RRR} \neq 0$, $H_{R\omega} \neq 0$, and that these have opposite signs at the bifurcation point.

Picking γ_0 to be a value of γ where the pitchfork occurs (where hysteresis and bifurcation curves intersect at $\pm\sqrt{3}$), we evaluate

$$H = (1+\gamma_0^2)R^3 - 2(\lambda+\gamma_0\omega)R^2 + (\lambda^2+\omega^2)R - \varepsilon_0^2 = 0, \tag{2.12}$$

$$H_R = 3(1+\gamma_0^2)R^2 - 4(\lambda+\gamma_0\omega)R + (\lambda^2+\omega^2) = 0, \tag{2.13}$$

$$H_{RR} = 6(1+\gamma_0^2)R - 4(\lambda+\gamma_0\omega) = 0, \tag{2.14}$$

$$H_\omega = 2\omega R - 2\gamma_0 R^2 = 0. \tag{2.15}$$

We note that using the above equation, it is clear that $\omega = \gamma_0 R$.

$$H_{R\omega} = 2\omega - 4\gamma_0 R. \tag{2.16}$$

Since $\omega = \gamma_0 R$, we see that $H_{R\omega} = -2\gamma_0 R < 0$ when $\varepsilon > 0$.

$$H_{RRR} = 6(1+\gamma_0^2) > 0. \tag{2.17}$$

So, these nondegeneracy conditions are always satisfied.

Finally, we check that the unfolding of the pitchfork in (γ, λ) space is a universal unfolding. To begin, we let $h(R) = H(R)$ evaluated with $\gamma = \sqrt{3}$ and $\lambda = \sqrt[3]{\frac{27}{4}}$ (i.e., tuned to the pitchfork bifurcation point). We must verify (see [9, p. 138, Proposition 4.4]) that

$$\det \begin{pmatrix} 0 & 0 & h_{R\omega} & h_{RRR} \\ 0 & h_{\omega R} & h_{\omega\omega} & h_{\omega RR} \\ H_\lambda & H_{\lambda R} & H_{\lambda\omega} & H_{\lambda RR} \\ H_\gamma & H_{\gamma R} & H_{\gamma\omega} & H_{\gamma RR} \end{pmatrix} \neq 0.$$

Taking the required derivatives, we find that the matrix has the form

$$D = \det \begin{pmatrix} 0 & 0 & 2\omega - 4\sqrt{3}R & 24 \\ 0 & 2\omega - 4\sqrt{3}R & 2R & -4\sqrt{3} \\ 2\lambda R - 2R^2 & 2\lambda - 4R & 0 & -4 \\ -2\omega R^2 + 2\gamma R^3 & -4\omega R + 6\gamma R^2 & -2R^2 & -4\omega + 12\gamma R \end{pmatrix}.$$

We must evaluate this at the bifurcation point, so we substitute in $\gamma = \sqrt{3}$ and $\lambda = \left(\frac{27}{4}\right)^{\frac{1}{3}}$. We see from [19] that to be on the hysteresis variety when $\gamma = \sqrt{3}$, we must have $R = \left(\frac{1}{4}\right)^{\frac{1}{3}}$. Finally, by (2.16), $\omega = \gamma R = \frac{\sqrt{3}}{4^{\frac{1}{3}}}$.

Evaluated at this point, the matrix has the form

$$D = \det \begin{pmatrix} 0 & 0 & -2^{1/3}\sqrt{3} & 24 \\ 0 & -2^{1/3}\sqrt{3} & 2^{1/3} & -4\sqrt{3} \\ 2^{2/3} & 2^{1/3} & 0 & -4 \\ 0 & \frac{\sqrt{3}}{2^{1/3}} & -\frac{1}{2^{1/3}} & 4\ 2^{1/3}\sqrt{3} \end{pmatrix}.$$

We compute the determinant of this matrix and find $D = -12\sqrt{3}2^{\frac{2}{3}} \neq 0$. A similar computation holds for $\gamma = -\sqrt{3}$. When $\gamma = -\sqrt{3}$, the determinant satisfies $D = (12\sqrt{3})2^{\frac{2}{3}} \neq 0$. The theorem follows. ■

So, we have seen that there is a pitchfork bifurcation when $\gamma = \pm\sqrt{3}$, and the unfolding afforded by variation of γ and λ is a universal unfolding. In Figure 4, we show the universal unfolding of the pitchfork. Portions of the bifurcation diagrams that are present in our system, but not local to the pitchfork bifurcation, are shown in red.

Finally, we note that the curves shown in Figure 4 provide the solution structure in the remaining regions of the bifurcation diagram shown in Figure 1.

2.2. Secondary Hopf bifurcation and Takens–Bogdanov varieties. It is proven in [20] that for any fixed value of γ, when λ is positive, the stable phase-locked solution to (2.1) near $\omega = 0$ will lose stability via a secondary Hopf bifurcation (or a Neimark–Sacker bifurcation) and give rise to toroidal dynamics (cf. Broer [5]). It is intuitive that when λ is positive and $|\omega|$ is sufficiently large, we may see two characteristic frequencies instead of a single phase-locked solution.

But, it is proven in [19] that for any fixed value of γ, there are no secondary Hopf bifurcations (for any value of ω) if γ is sufficiently large. So, in Figure 1, it is not clear what should

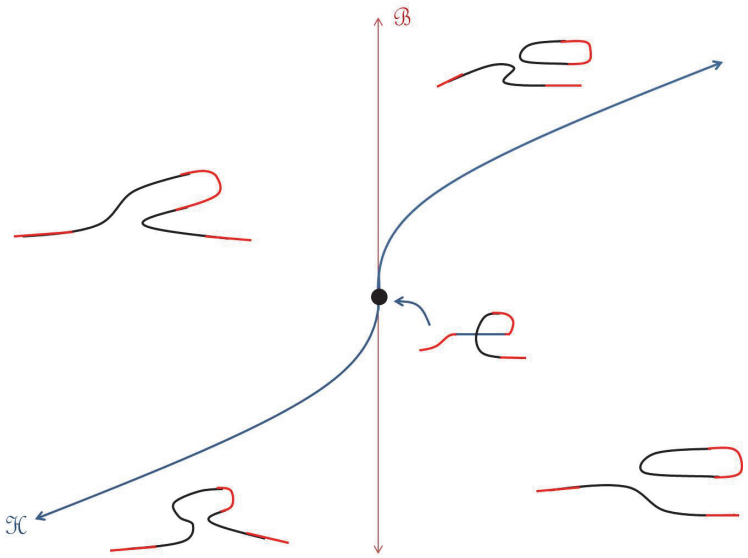

Figure 4. *Universal unfolding of pitchfork with portions of the bifurcation diagrams that are present in our system, but not local to the pitchfork bifurcation, shown in red.*

happen to these secondary Hopf bifurcations if we tune the system close to the γ axis with $\lambda > 0$ and begin increasing λ. So, we begin to investigate the fate of the secondary Hopf bifurcations. We will find that the secondary Hopf bifurcations terminate at Takens–Bogdanov points and occur along varieties in (λ, γ) space shown in Figure 5.

If one considers (2.4) as a vector field in $\mathbb{R}^2$ by the normal identification of $\mathbb{R}^2$ with $\mathbb{C}$, the eigenvalues of the derivative of this mapping, as shown in [20], are given by

$$\Lambda^2 - 2(\lambda - 2R)\Lambda + H_R. \tag{2.18}$$

It follows that the determinant of a fixed point is given by H_R, and the trace is given by $2(\lambda - 2R)$. We further note that, as shown by Zhang and Golubitsky in [20], the eigenvalue crossing conditions of the secondary Hopf bifurcation points discussed above are always satisfied ($R_\omega = \lambda - 2R = 0$ has no solutions except when $H_R < 0$). So, there is always a unique branch of periodic solutions (branches of tori in stationary coordinates) emanating from the secondary Hopf bifurcation points. We also note, as shown in [20], that there are two Takens–Bogdanov varieties (satisfying $H = H_R = \lambda - 2R = 0$) where $\mathcal{TB}^{\pm}$ are given by

$$\lambda^3 = 4\varepsilon^2 \left(1 \pm \frac{\gamma}{\sqrt{1+\gamma^2}}\right).$$

So, we may add these two curves to the diagram in Figure 1 to obtain Figure 5 by setting $\varepsilon = 1$ to produce the dynamics of (2.3). Recall that the shapes of the forced response curves that correspond to regions in Figure 5 are known, as they are shown in Figure 1.

2.3. The stability of solutions. In this section, our goal will be to determine the stability of the periodic solutions corresponding to points on the forced response curves in each region of Figure 5 to obtain Figure 6.

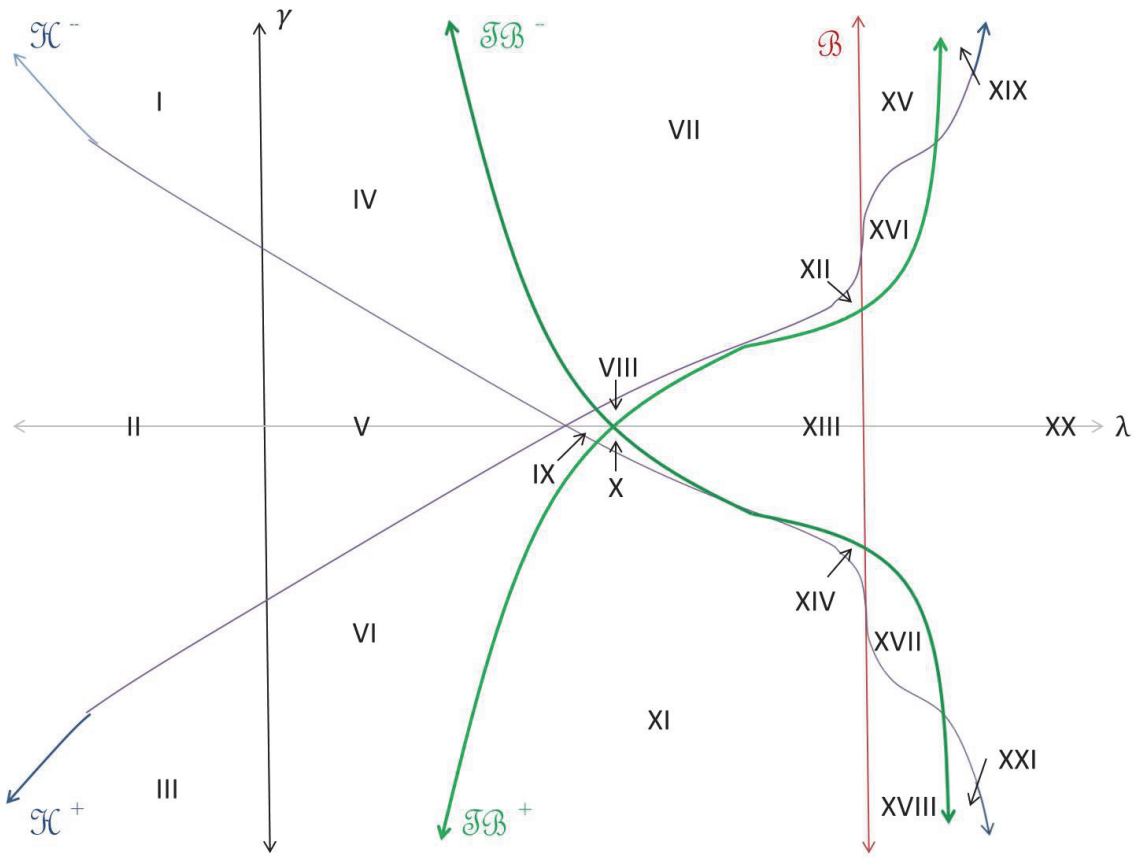

Figure 5. *Solution structure with stability: Figure 1 with Takens–Bogdanov curves added. Since regions also reflect stability, crossing the γ axis now results in changing regions. Numbered regions correspond to forced response curves in Figure 6.*

We are aided by the observation that crossing a Takens–Bogdanov variety will result in a secondary Hopf bifurcation colliding with a saddle node point and disappearing as we move from left to right (as discussed previously). However, as we traverse parameter space in Figure 5, it will sometimes occur that as we cross a Takens–Bogdanov variety, there will be multiple secondary Hopf bifurcations and/or multiple saddle node bifurcations, making it difficult to determine the stabilities on the resulting curve. Toward these ends, we find the following result useful.

Proposition 2.5. *For any fixed value of γ if we choose λ tuning the system to a Takens–Bogdanov bifurcation variety, then the following hold.*

For $\mathcal{TB}^+$, at the bifurcation point,

$$\frac{\partial^2\omega}{\partial R^2} < 0 \text{ for } \gamma < \frac{1}{\sqrt{3}} \quad \text{and} \quad \frac{\partial^2\omega}{\partial R^2} > 0 \text{ for } \gamma > \frac{1}{\sqrt{3}}.$$

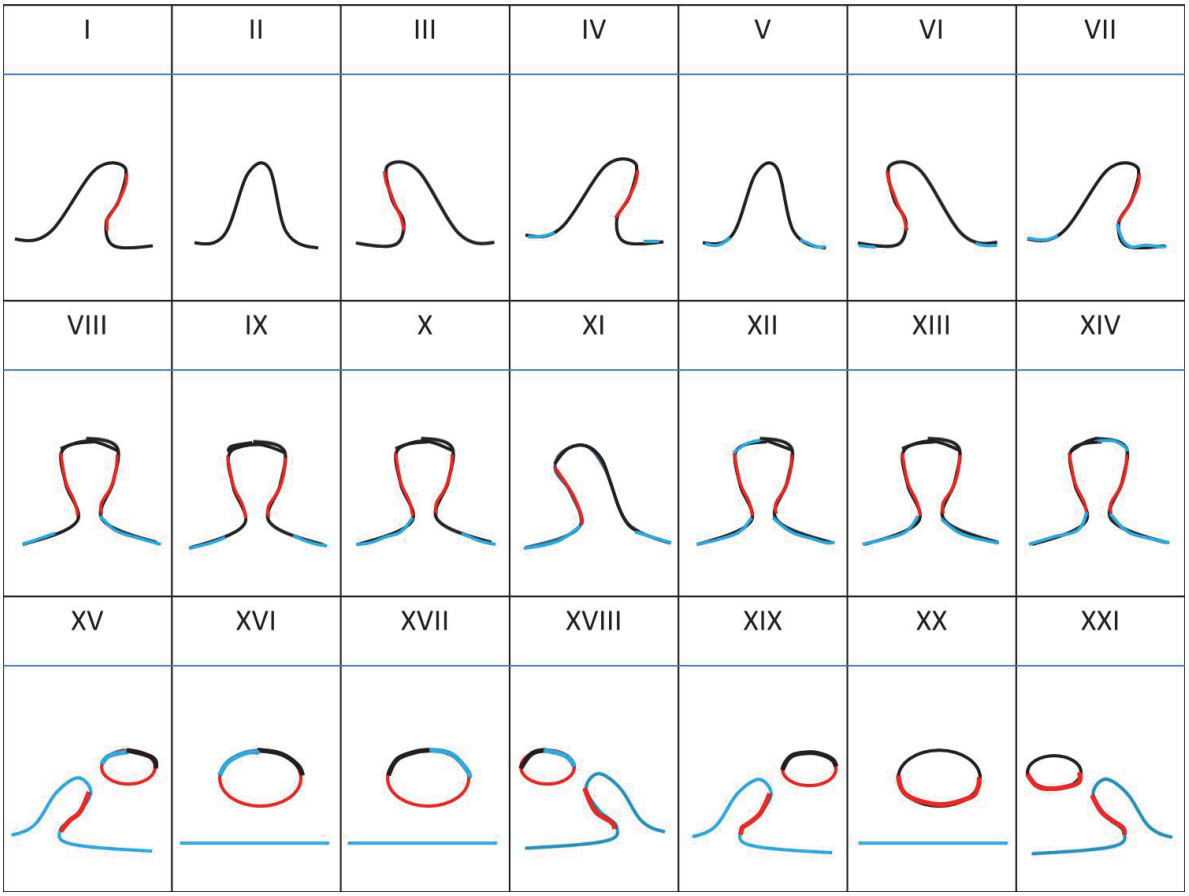

Figure 6. *Forced response curves (representing the radii of steady state equilibria—in rotating coordinates) to (2.3). The numbering of the diagrams corresponds to parameter regions shown in Figure 5. Here, blue lines represent unstable equilibria, black lines represent stable equilibria and red lines represent saddle stability. Hence, the incidence of a blue or red curve with a black curve represents a saddle node bifurcation and the incidence of a black and blue curve represents a secondary Hopf bifurcation.*

But, for $\mathcal{TB}^-$, at the bifurcation point,

$$\frac{\partial^2\omega}{\partial R^2} < 0 \text{ for } \gamma < -\frac{1}{\sqrt{3}} \quad \text{and} \quad \frac{\partial^2\omega}{\partial R^2} > 0 \text{ for } \gamma > -\frac{1}{\sqrt{3}}.$$

Proof. We begin by fixing $\gamma = \gamma_0$ and tuning λ to λ_{TB}, the TB^+ bifurcation point. We also call the ω value where the TB^+ bifurcation occurs ω_{TB} and the R value R_{TB}. Setting $H(R) = 0$ at (γ_0, λ_{TB}), we find

$$0 = (1+\gamma_0^2)R^3 - 2(\lambda_{TB} + \gamma_0\omega)R^2 + (\lambda_{TB}^2 + \omega^2)R - 1.$$

Taking a partial derivative with respect to R, we find

$$0 = 3(1+\gamma_0^2)R^2 - 4(\lambda_{TB} + \gamma_0\omega)R + (\lambda_{TB}^2 + \omega^2) + 2(\omega R - \gamma_0 R^2)\frac{\partial\omega}{\partial R}.$$

Taking a second partial derivative with respect to R,

$$6(1+\gamma_0^2)R - 4(\lambda_{TB}+\gamma_0\omega) - 4\gamma_0 R\frac{\partial\omega}{\partial R} + 2(\omega - 2\gamma_0 R)\frac{\partial\omega}{\partial R} + 2(\omega R - \gamma_0 R^2)\frac{\partial^2\omega}{\partial R^2} = 0.$$

However, since the Takens–Bogdanov bifurcations occur at saddle nodes, $\frac{\partial\omega}{\partial R}$ must be zero at these points. Thus, simplifying and evaluating at ω_{TB} and R_{TB},

$$\frac{\partial^2\omega}{\partial R^2} = \frac{2(\lambda_{TB}+\gamma_0\omega_{TB}) - 3(1+\gamma_0^2)R_{TB}}{\omega_{TB}R_{TB} - \gamma_0 R_{TB}^2}. \tag{2.19}$$

Finally, eliminating $R_{TB} = \frac{\lambda_{TB}}{2}$, $\omega_{TB} = \frac{4+(\gamma_0^2-1)\lambda_{TB}^3}{2\gamma_0\lambda_{TB}^2}$, and $\lambda_{TB} = (4 + \frac{4\gamma_0}{\sqrt{\gamma_0^2+1}})^{\frac{1}{3}}$ (see [19] for a derivation of these expressions), we may rewrite the right-hand side of (2.19) as

$$\left(\frac{2}{1-\frac{\gamma_0}{\sqrt{\gamma_0^2+1}}}\right)^{\frac{1}{3}} \gamma_0(\gamma_0^2+1) + (\gamma_0^2-1)\sqrt{\gamma_0^2+1}. \tag{2.20}$$

We wish to find the zeros of (2.20). To do this, we demand equality of squares of both terms in the sum and then solve for $\gamma_0 = \pm\frac{1}{\sqrt{3}}$. Substituting this back into (2.20), we find that $\frac{1}{\sqrt{3}}$ is the only solution. A brief inspection shows that the sign of $\frac{\partial^2\omega}{\partial R^2}$ changed from negative to positive at this zero. Thus, the proposition is established for $\mathcal{TB}^+$. A similar analysis establishes the result for $\mathcal{TB}^-$. ■

We now proceed to determine the stability of various regions in Figure 5. First, using Proposition 2.5, we can determine the stability of Region 7 that results from crossing $\mathcal{TB}^-$ from Region 4, and we can determine the stability of Region 11 that results from crossing $\mathcal{TB}^+$ from Region 6. Given that there are no secondary Hopf bifurcations in Region 20, using Proposition 2.5, we may determine the stability of Region 16 by passing from Region 20 to Region 16, crossing the $\mathcal{TB}^+$ line. Similarly, the stability of Region 17 is clear crossing the $\mathcal{TB}^-$ curve from Region 20. Additionally, the stabilities of Regions 12, 13, and 14 are clearly obtained by crossing the simple bifurcation curve from Regions 16, 20, and 17, respectively.

In order for Region 4 (by crossing $\mathcal{H}^+$) and Region 6 (by crossing $\mathcal{H}^-$) to match in Region 9, the stability of Region 9 must be as shown in Figure 5. Given the stability in Region 9, Proposition 2.5 may be used to determine the stabilities in Regions 8 and 10. In order for Regions 16 (by crossing $\mathcal{H}^+$) and 7 (by crossing $\mathcal{B}$) to match in Region 15, the stability of Region 15 must be as shown in Figure 5. Similarly, we can find the stability of Region 18 by matching Regions 11 and 17. Finally, the matching Regions 15 and 20 dictate the stability of Region 19, and Regions 18 and 20 dictate the stability of Region 21.

2.4. Degenerate bifurcations. A quick investigation of global phenomena in the system (2.3) suggests that higher codimension degeneracies must be missing from Figure 5. For example, we know that near the Takens–Bogdanov bifurcations, saddle connections must also be present where there are secondary Hopf bifurcations. However, it is easy to see that these saddle connections cannot be everywhere to the "left" of the Takens–Bogdanov varieties in Figure 5. (Note that some regions of parameter space do not even have points with saddle

stability.) In this section, we will show that there are points in Figure 5 where the Takens–Bogdanov bifurcations are elliptically degenerate. Local to those points, we will find curves of degenerate (change of criticality) secondary Hopf bifurcations and a curve of *SNL* bifurcations (homoclinic connections to a degenerate saddle point), where the saddle connections terminate. Adding these curves to Figure 5 will result in Figure 2 shown in the introduction.

2.4.1. Degenerate Takens–Bogdanov bifurcation. Recall that, by introducing a formal, smooth coordinate change, the system (2.4), tuned to a Takens–Bogdanov bifurcation point, can be put into the form

$$\begin{aligned}\dot{x}_0 &= x_1\\ \dot{x}_1 &= \sum_{k=2}^{\infty}(a_k x_0^k + b_k x_0^{k-1} x_1).\end{aligned}$$

Recall that in the nondegenerate case (when $a_2 b_2 \neq 0$), a Takens–Bogdanov bifurcation can be put into the normal form

$$\begin{aligned}\dot{x_0} &= x_1,\\ \dot{x_1} &= a_2 x_0^2 + b_2 x_0 x_1\end{aligned}$$

and can be unfolded by two parameters μ_1 and μ_2 via

$$\begin{aligned}\dot{x_0} &= x_1,\\ \dot{x_1} &= \mu_1 + \mu_2 x_1 + a_2 x_0^2 + b_2 x_0 x_1.\end{aligned}$$

Hence, there is a natural classification of two types of degenerate (codimension 3) Takens–Bogdanov singularities. If $b_2 = 0$, but $a_2 b_4 \neq 0$, this case is called a "cusp of codimension 3." Generic three-dimensional unfoldings of this system have bifurcation diagrams which are locally topologically equivalent to those of the canonical family

$$\begin{aligned}\dot{x_0} &= x_1,\\ \dot{x_1} &= \mu_1 + \mu_2 x_1 + \mu_3 x_0 x_1 + a_2 x_0^2 + b_4 x_0^3 x_1.\end{aligned}$$

Alternatively, the following conjecture is proposed by Dumortier et al. in [7].

Conjecture 2.6. *If $a_2 = 0$, $b_2 a_3 \neq 0$, then generic three-parameter unfoldings of the system have bifurcation diagrams that are locally topologically equivalent to those of the "standard family"*

$$\begin{aligned}\dot{x_0} &= x_1,\\ \dot{x_1} &= \mu_1 + \mu_2 x_0 + \mu_3 x_1 + a_3 x_0^3 + b_2 x_0 x_1 + c_3 x_0^2 x_1,\end{aligned}$$

where $c_3 = b_3 - \frac{3 b_2 a_4}{5 a_3}$.

The generic unfoldings obtained by variation of $\vec{\mu}$ in the standard family depends on the other normal form coefficients in this case. Assuming, without loss of generality, that $b_2 > 0$ (we may change coordinates via $\vec{x} \to -\vec{x}$ if $b_2 < 0$), the standard family has three topologically

distinct unfoldings. When $a_3 > 0$, the degenerate Takens–Bogdanov singularity is said to have saddle type. When $a_3 < 0$, two possibilities remain. If $b_2^2 + 8a_3 < 0$ (and the nondegeneracy condition $c_3 \neq 0$ holds), then the singularity is said to be of focus type. But, if $b_2^2 + 8a_3 > 0$, the singularity is said to be of elliptic type. Note that the complete proof of Conjecture 2.6 is obtained only in the case of saddle-type singularities but is believed to be true in all three cases [14].

Formulas for the coefficients $\{a_n\}$ and $\{b_n\}$ were derived by Kuznetsov in [14]. In [19], these formulas are applied to show that for $TB^{\pm}$, $a_2 = 0$ only when $\gamma = \pm 1/\sqrt{3}$, respectively. Thus, there are degenerate Takens–Bogdanov bifurcations at this point. Furthermore, $b_2 a_3 \neq 0$ for any value of γ, so we know that there are no other degeneracies. That is, we have found that there are exactly two codimension 3 degenerate Takens–Bogdanov bifurcations. It was also shown that $b_2^2 + 8a_3 \approx 1.04396 > 0$. Hence, the degenerate Takens–Bogdanov bifurcations discovered were of elliptic type. Note that these values of γ correspond exactly to the intersection of the $\mathcal{H}$ and $\mathcal{TB}$ varieties.

2.4.2. Degenerate secondary Hopf bifurcation. From the unfolding of the codimension 3 elliptically degenerate Takens–Bogdanov bifurcation found in [7], we see that there should be a ray of degenerate (change of criticality) Hopf bifurcations local to these points. (We note that the translation from the distinguished parameter language of this paper to the unfolding in [7] is not trivial, and the details are discussed in [19].)

Tuning the system to the secondary Hopf bifurcation points and computing the real part of the cubic coefficient of the normal form secondary Hopf bifurcations (there are well known formulas for this; see, for example, [6] or [12]), we can determine the criticality of the secondary Hopf bifurcations. This calculation, performed in [19], yields the curves $\mathcal{CC}^{\pm}$ shown in Figure 2.

2.4.3. Homoclinic connections and SNL varieties. As we mentioned before, there are homoclinic orbits local to the Takens–Bogdanov varieties. So, it is clear that some regions of parameter space (shown in Figure 2) should have saddle connections, but others (for example, regions with no saddle points) should not. It is not clear, however, which regions of parameter space should have homoclinic orbits present, which should not, and how the system (2.4) should transition between these two possibilities.

Using the unfolding of the degenerate Takens–Bogdanov singularity in [7], one finds that there should be a curve of SNL bifurcations (saddle connections to a degenerate saddle point) local to the degenerate Takens–Bogdanov singularities. It is not obvious how to parameterize these curves. However, it is clear that they should remain to the left of the $\mathcal{TB}$ varieties and to the right of the γ axis—because there should be secondary Hopf bifurcations present on the forced response curve if there are saddle connections. Also, the $\mathcal{SNL}$ varieties should stay to the right of the $\mathcal{H}$ varieties, since there should be a saddle point present to have a saddle connection. Note that in Figure 2, the $\mathcal{SNL}$ curve is drawn as never intersecting the $\mathcal{CC}$ varieties. This is not known to be true in general.

These observations justify the placement of the $\mathcal{SNL}$ curves to the left of the degenerate Takens–Bogdanov bifurcations in Figure 2. However, we must consider how they emanate moving to the right—in the direction of increasing λ. It is clear that the $\mathcal{SNL}$ curve must bisect the region between the hysteresis and the Takens–Bogdanov bifurcation varieties (consistent

with our arguments on the left side). However, $\mathcal{SNL}$ cannot cross the variety $\mathcal{B}$ since the saddle node bifurcation point (the degenerate saddle point) possessing a homoclinic connection will disappear after the bifurcation. If it touches the bifurcation variety and terminates without crossing, then increasing λ across the bifurcation variety could eliminate a homoclinic orbit without crossing the $\mathcal{SNL}$ bifurcation variety. Thus, the $\mathcal{SNL}$ bifurcation curve must terminate at the pitchfork bifurcation point. In fact, we can see that the homoclinic orbit must be local to the *SNL*/pitchfork bifurcation. If it were not, then the center manifold of the pitchfork bifurcation (which includes either the stable or the unstable manifold of the saddle point) would contain the entire homoclinic cycle. But this cannot be the case because then there would be an additional node on the homoclinic cycle. Thus, we arrive at the diagram shown in Figure 2.

2.5. Forced response curves. With this information, we can add all of the detail to the forced response curves in Figures 2 and 3. Note that we have shown the criticality of the secondary Hopf bifurcation and drawn in a curve representing the amplitude of the emanating tori (periodic orbits in rotating coordinates). Note that we have also encoded the stability of the tori and the stability of the saddle connections, which are dictated by the criticality of the secondary Hopf bifurcations. We also note that, as is indicated in the unfolding of the degenerate Takens–Bogdanov bifurcation in [7], tori terminate via homoclinic bifurcation prior to crossing the $\mathcal{SNL}$ variety and via cycle blowup after crossing the variety.

3. Discussion. The results of this paper begin to classify the dynamics of periodically forced Hopf bifurcation with the forcing frequency as a distinguished parameter. To apply this research to particular model equations, one must tune to a Hopf bifurcation point, perform a center manifold reduction, and compute the normal form parameter γ. Then, one uses Figures 2 and 3 to understand which transitions in the forced response curve one should expect to see as model parameters are varied.

The results are also limited by the requirement that we examine only small amplitude sinusoidal forcing. There are also small regions of parameter space (when the system is tuned near a bifurcation variety) where the dynamics of the system may be arbitrarily complicated, and large regions of parameter space (with saddle connections present) where chaotic dynamics may generically occur. Some comments on the generality of the results presented here are given in Wiser [19]. Points that are discussed include the breaking of normal form, the third order truncation, and separable forcing.

This research could be extended by looking at networks of systems near Hopf bifurcations. It has already been suggested that the dynamics of exceptionally simple networks of systems near Hopf bifurcations may have surprising dynamics (see [11, 10]) or play a role in physiological models (see [3], for example).

REFERENCES

[1] V.I. Arnold, *Small divisors* I: *On mappings of the circle onto itself*, Izv. Akad. Nauk SSSR Ser. Mat., 25 (1961), pp. 21–86 (in Russian); Amer. Math. Soc. Trans., 46 (1965), pp. 213–284.

[2] V.I. Arnold, *Geometrical Methods in the Theory of Ordinary Differential Equations*, Springer, New York, 1988.

[3] G. Baier and M. Müller, *Frequency selective induction of excitation waves near sub and supercritical Hopf bifurcation*, Phys. Lett. A, 330 (2004), pp. 350–357.
[4] J. Balakrishnan and B. Ashok, *The role of Hopf bifurcation dynamics in sensory processes*, J. Theoret. Biol., 265 (2010), pp. 126–135.
[5] H.W. Broer, *Resonance and fractal geometry*, Acta Appl. Math., 120 (2012), pp. 61–86.
[6] S.-N. Chow, C. Li, and D. Wang, *Normal Forms and Bifurcation of Planar Vector Fields*, Cambridge University Press, Cambridge, UK, 1994.
[7] F. Dumortier, R. Roussarie, J. Sotomayor, and H. Zoladek, *Bifurcations of Planar Vector Fields: Nilpotent Singularities and Abelian Integrals*, Springer, New York, 1991.
[8] J.-M. Gambaudo, *Perturbation of a Hopf bifurcation by an external time-periodic forcing*, J. Differential Equations, 57 (1985), pp. 172–199.
[9] M. Golubitsky and D. Schaeffer, *Singularities and Groups in Bifurcation Theory, Vol.* 1, Appl. Math. Sci. 51, Springer-Verlag, New York, 1985.
[10] M. Golubitsky and C. Postlethwaite, *Feed-forward networks, center manifolds, and forcing*, Discrete Contin. Dynam. Syst Ser. A, 32 (2012), pp. 2913–2935.
[11] M. Golubitsky, C. Postlethwaite, L.-J. Shiau, and Y. Zhang, *The feed-forward chain as a filter amplifier motif*, in Coherent Behavior in Neuronal Networks, K. Josic, M. Matias, R. Romo, and J. Rubin, eds., Springer, New York, 2009, pp. 95–120.
[12] J. Guckenheimer and P. Holmes, *Nonlinear Oscillations, Dynamical Systems, and Bifurcations of Vector Fields*, Appl. Math. Sci. 42, Springer-Verlag, New York, 1983.
[13] A. Hudspeth, *Making an effort to listen: Mechanical amplification in the ear*, Neuron, 59 (2008), pp. 530–545.
[14] Y.A. Kuznetsov, *Practical computation of normal forms on center manifolds at degenerate Bogdanov-Takens bifurcations*, Internat. J. Bifur. Chaos Appl. Sci. Engrg., 15 (2005), pp. 3535–3546.
[15] N.J. McCullen, T. Mullin, and M. Golubitsky, *Sensitive signal detection using a feed-forward oscillator network*, Phys. Rev. Lett., 98 (2007), 254101.
[16] A. Mees and L. Chua, *The Hopf bifurcation theorem and its applications to nonlinear oscillations in circuits and systems*, IEEE Trans. Circuits Syst., 26 (1979), pp. 235–254.
[17] R.E. Simpson, *Introductory Electronics for Scientists and Engineers*, Allyn and Bacon, Boston, 1987.
[18] J. Tyson, *Computational cell biology*, Science, 214 (1981), 1350.
[19] J. Wiser, *Harmonic Resonance Dynamics of the Periodically Forced Hopf Oscillator*, Ph.D. thesis, The Ohio State University, Columbus, OH, 2013.
[20] Y. Zhang and M. Golubitsky, *Periodically forced Hopf bifurcation*, SIAM J. Appl. Dyn. Syst., 10 (2011), pp. 1272–1306.